LiFe(MoO$_4$)$_2$ as a Novel Anode Material for Lithium-Ion Batteries

Nan Chen,[†] Ye Yao,[†] Dongxue Wang,[†] Yingjin Wei,[†] Xiaofei Bie,*[,†] Chunzhong Wang,[†,‡] Gang Chen,[†,‡] and Fei Du*[,†]

[†]Key Laboratory of Physics and Technology for Advanced Batteries (Ministry of Education), College of Physics, [‡]State Key Laboratory of Superhard Materials, Jilin University, Changchun 130012, People's Republic of China

ABSTRACT: Polycrystalline LiFe(MoO$_4$)$_2$ is successfully synthesized by solid-state reaction and examined as anode material for lithium-ion batteries in terms of galvanostatic charge−discharge cycling, cyclic voltammograms (CV), galvanostatic intermittent titration technique (GITT), and electrochemical impedance spectroscopy (EIS). The LiFe-(MoO$_4$)$_2$ electrode delivers a high capacity of 1034 mAh g^{-1} at a current density of 56 mA g^{-1} between 3 and 0.01 V, indicating that nearly 15 Li$^+$ ions are involved in the electrochemical cycling. LiFe(MoO$_4$)$_2$ also exhibits a stable capacity of 580 mAh g^{-1} after experiencing irreversible capacity loss in the first several cycles. Moreover, the Li-ion storage mechanism for LiFe(MoO$_4$)$_2$ is suggested on the basis of the ex situ X-ray diffraction (XRD) and high-resolution transmission electron microscopy (HRTEM) at different insertion/extraction depths. A successive structural transition from triclinic structure to cubic structure is observed, and the tetrahedral coordination of Mo by oxygen in LiFe(MoO$_4$)$_2$ changes to octahedral coordination in Li$_2$MoO$_3$, correspondingly. When being discharged to 0.01 V, the active electrode is likely to be composed of Fe and Mo metal particles and amorphous Li$_2$O due to the multielectron conversion reaction. The insights obtained from this study will benefit the design of new anode materials for lithium-ion batteries.

KEYWORDS: lithium-ion battery, anode materials, lithium molybdate, electrochemical properties
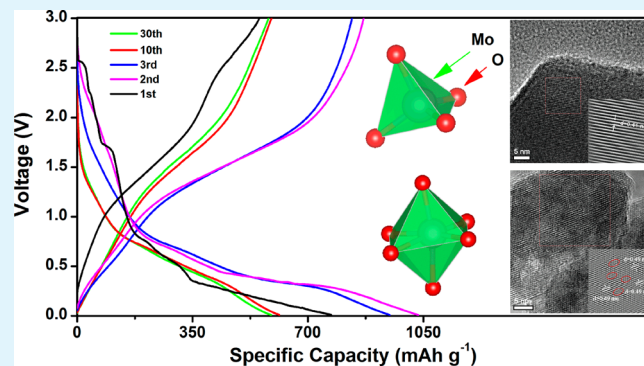
INTRODUCTION

With the growing demand for advanced portable electronic devices and electric vehicles, research on lithium-ion batteries has become mainstream in the field of clean and renewable energy.[1,2] The limited theoretical capacity of graphite (372 mAh g^{-1}) as anode material has prompted an intensive search for alternative materials that can intercalate more lithium ions at low potential, such as MnO,[3] Fe$_3$O$_4$,[4] SnO$_2$,[5] GeO$_2$,[6] and TiO$_2$.[7,8] Molybdenum has been considered as one of the prospective anode materials due to its high flexibility in accepting a wide range of oxidation states from 0 to +6.[9] For example, MoO$_3$ as a well-known anode material exhibits a high capacity of 940 mAh g^{-1}.[10] Some complex molybdenum oxides, such as CoMoO$_4$, ZnMoO$_4$, or FeMoO$_4$, can also show a reversible capacity of more than 500 mAh g^{-1}.[11] On the basis of the conversion mechanism, Mo^{6+} ions in both MoO$_3$ and MMoO$_4$ will convert to Mo metal nanoparticles during deep discharge, and MoO$_3$ reforms upon charging to 3 V.[10,11]

Utilization of cathode materials as negative electrodes is found to be very interesting in recent research.[12,13] LiFePO$_4$ exhibits an initial discharge capacity of about 650 mAh g^{-1}, and Fe and Li$_3$PO$_4$ nanograins are formed when discharged to 0.005 V.[12] A purely capacitive energy storage behavior is suggested in the Fe/Li$_3$PO$_4$ nanocomposites, different from the traditional secondary batteries. Li$_2$FeSiO$_4$ can also deliver an initial discharge capacity of 880 mAh g^{-1} and stabilize at nearly 500 mAh g^{-1}, much higher than that of commercial graphite.

Transition metal nanoparticles, Fe, and silica are found to be the final products at the discharge potential of 0 V. The Li storage mechanism in Li$_2$FeSiO$_4$, however, needs more detailed experiments.[13]

LiFe(MoO$_4$)$_2$, which belongs to triclinic symmetry (space group $P1$), is composed with separated layers of [LiO$_6$] monocapped trigonal bipyramids and [FeO$_6$] octahedra and is connected by layers of isolated [MoO$_4$] tetrahedra.[14] Movement of Li$^+$ ions along a one-dimensional channel direction is expected during the electrochemical cycles. A recent study on the Polyanion-type LiFe(MoO$_4$)$_2$ as cathode finds a reversible capacity of 180 mAh g^{-1} in the voltage window of 3.0−1.0 V.[15] One interesting feature is that the electrochemical process involves two redox couples: Fe^{2+}/Fe^{3+} and Mo^{4+}/Mo^{6+} at 2.6 and 1.8 V,[15] respectively. Note that polyanion-type compounds usually show good cycling performance because the strong binding energy of polyanion could stabilize the crystal structure.[16,17] The second discharge plateau at 1.8 V via Mo^{6+}/Mo^{4+}, however, might suggest the instability of [MoO$_4$] tetrahedra and a complete structural transition is expected, especially at low discharge potential.

In this work, we, for the first time, report a comprehensive study on the electrochemical properties of LiFe(MoO$_4$)$_2$ as

anode in the voltage window of 3.0–0.01 V by galvanostatic charge–discharge cycling, CV, GITT, and EIS. The electrochemical process is also explained on the basis of the conversion mechanism by ex situ X-ray diffraction (XRD) and high-resolution transmission electron microscopy (HRTEM). Our study provides significant insight into the design of and research on the new anode material with multielectron reaction mechanism.

■ EXPERIMENTAL SECTION

Polycrystalline $LiFe(MoO_4)_2$ was synthesized by solid-state reaction. Stoichiometric amounts of Li_2CO_3 (Aldrich 99%), Fe_2O_3 (Aldrich 99%), and MoO_3 (Aldrich 99.5%) were mixed together according to Li/Fe/Mo = 1:1:2 using ethanol in an agate mortar for 2 h and then pressed into a pellet. After calcinations in air for 24 h with an intermediate grinding, the resulting yellow powder $LiFe(MoO_4)_2$ was obtained. The XRD pattern was recorded in the 2θ range of 10−50° at a scanning rate of 2°/min using Bruker D8 with Cu Kα source. The particle sizes and morphologies of the obtained samples were observed using a Hitachi SU8020 type scanning electron microscope (SEM). The microstructure was studied using an FEI Tecnai G2 type transmission electron microscope (TEM).

Electrochemical experiments were carried out using 2032-type coin cells. A typical electrode was composed of $LiFe(MoO_4)_2$ active material (70 wt %), carbon black conductive additive (20 wt %), and polyvinylidene fluoride binder (PVDF, 10 wt %) dissolved in N-methylpyrrolidone (NMP). First, the slurry mixture was pasted on a copper foil and dried at 120 °C for 12 h in a vacuum oven. Each electrode, 8×8 mm^2 in size, contained about 3 mg of active material. Then, the cathode and anode electrodes were separated by Celgard 2400 membrane. The electrolyte was 1 M lithium hexafluorophosphate ($LiPF_6$) dissolved in ethylene carbonate (EC), dimethylcarbonate (DMC), and ethyl methyl carbonate (EMC) with EC/DMC/EMC = 1:1:8 by volume ratio. Galvonostatic charge–discharge cycling was performed on a Land-2001A (Wuhan, China) automatic battery tester. Data of cyclic voltammetry (CV), GITT, and EIS were recorded on a VSP multichannel potentiostatic–galvanostatic system (Biologic, France). CV curves were collected at a scanning rate of 0.1 mVs^{-1}. For the GITT measurement, the battery cell was discharged with a constant current flux for a given time followed by an open-circuit stand for a specified time interval. The impedance spectra were recorded by applying an AC voltage of 5 mV in the frequency range from 1 MHz to 1 mHz.

■ RESULTS AND DISCUSSIONS

Figure 1 shows the XRD pattern for the as-prepared $LiFe(MoO_4)_2$ by solid-state reaction. All the diffraction peaks can be indexed on the basis of space group $P1$, and no impurity phase can be found. The lattice constants are calculated to be a = 6.7811 Å, b = 7.1802 Å, c = 7.2904 Å, α = 90.77°, β = 110.40°, and γ = 105.12°, which are consistent with the previous report.[14] The sample is well-crystallized, as shown in the inset of Figure 1, with the average particle size of 3–5 μm after solid-state reaction.

Galvanostatic charge–discharge cycling for as-prepared $LiFe(MoO_4)_2$ is carried out in the voltage range of 3–0.01 V at a current density of 56 mA g^{-1}, as shown in Figure 2. Two flat plateaus can be observed in the first discharge curve, located at 2.57 and 1.74 V, corresponding to the two reduction reactions of Fe^{3+}/Fe^{2+} and Mo^{6+}/Mo^{4+}, respectively.[15] At low voltage, the discharge curve becomes smooth, with no sign of plateaus, and the first discharge capacity can reach 771 mAh g^{-1}. After the first discharge, the flat plateaus at 2.57 and 1.74 V disappear in the following cycles, suggesting an irreversible structural transition. Note that the second discharge capacity shows a high capacity of 1034 mAh g^{-1}, which corresponds to
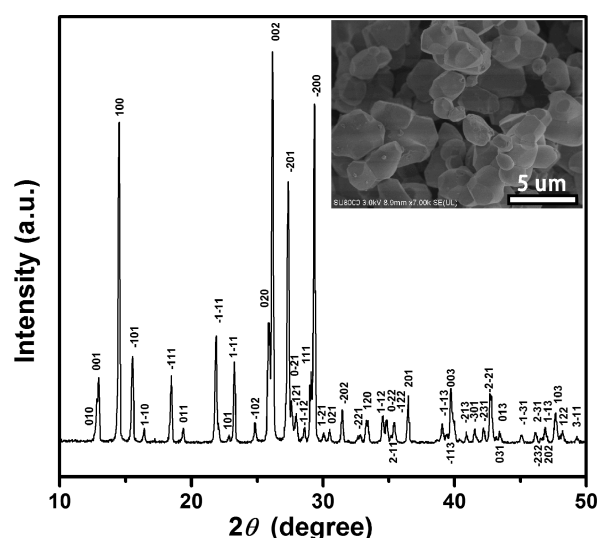

Figure 1. X-ray diffraction pattern of $LiFe(MoO_4)_2$. (Inset) SEM image of the as-prepared material.

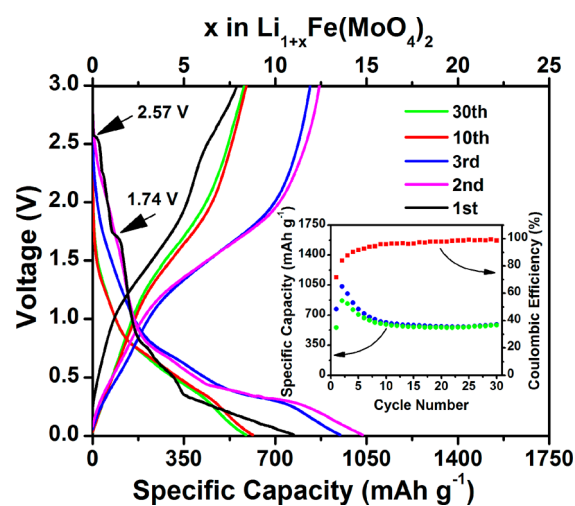**Figure 2.** Galvanostatic charge–discharge curves of $LiFe(MoO_4)_2$ between 3.0 and 0.01 V at a constant current density of 56 mA g^{-1}. (Inset) Cycle performance and Coulombic efficiency for 30 cycles.

an insertion of nearly 15 Li$^+$ ions and is consistent with the theoretical capacity of $LiFe(MoO_4)_2$ based on the conversion mechanism. The higher capacity of the second discharge than that of the first discharge can be attributed to the incomplete electrochemical reaction because of the large particle size and inadequate contact with electrolyte. The cycle performance and Coulombic efficiency of $LiFe(MoO_4)_2$ are also displayed in the inset of Figure 2. The capacity drops at the beginning and stabilizes at about 580 mAh g^{-1} after 30 cycles. The irreversible capacity loss in the first several cycles is observed due to the formation of solid electrolyte interfacial layer (SEI) and the decomposition of electrolyte. The poor electrical/ionic conductivity of resultant during the electrochemical process may also cause the irreversible lithium loss.[18,19] To improve the irreversible capacity, methods such as surface modification using carbon or graphene[18−20,23,25,31] are proposed because the active materials somehow cannot effectively release the large strain caused by volume expansion. Carbon/graphene coating would also decrease the resistance for lithium ion to reach the core of active materials.

Figure 3 shows the CV plots of $LiFe(MoO_4)_2$ electrodes at a scan rate of 0.1 mV s^{-1} vs Li/Li$^+$ between 3 and 0.01 V. There
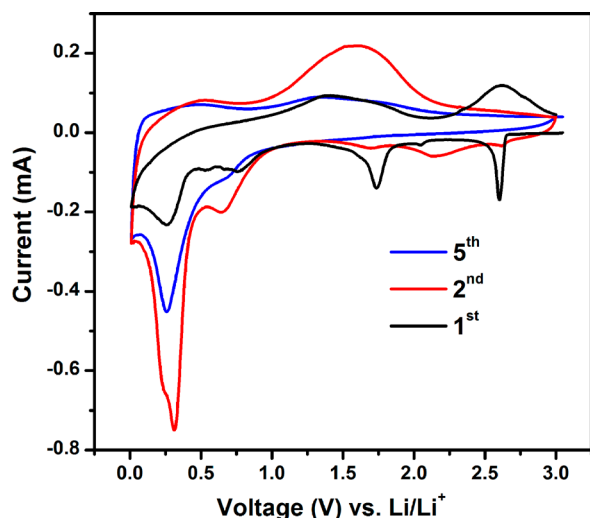

Figure 3. Cyclic voltammograms of $LiFe(MoO_4)_2$ electrode at a scan rate of 0.1 mV s^{-1}.

are two clear reduction peaks at 2.60 and 1.74 V in the first cathodic scan, which is associated with the initial reduction of Fe^{3+} to Fe^{2+} and Mo^{6+} to Mo^{4+}, respectively.[21,22] As the scan voltage drops, two reduction peaks are observed at 0.76 and 0.26 V, due to the reduction to Fe^0 and Mo^0 metal nanoparticles and the formation of solid electrolyte interface (SEI). In previous studies, similar reduction peaks below 1 V have been found in some simple transition metal oxides such as Fe_3O_4[23] and MoO_2[24] with conversion reaction, which provides a reversible electrochemical reaction of lithium ions. More importantly, such low-voltage CV peaks maintains after the first cycle, indicating that conversion mechanism will determine the electrochemical behavior of the anode after the first cycle. In the anodic scan, the reversible oxidation peak of Fe^0 to Fe^{3+} and Mo^0 to Mo^{6+} is around 1.45 V. However, the reduction peaks between Fe and Mo are hard to distinguish because the Fe and Mo oxides have similar oxidation/reduction peaks.[25−29] In addition, due to the unreacted $LiFe(MoO_4)_2$, a pair of redox peaks at 2.62 and 2.13 V is observed in the first anodic and second cathodic scan, respectively, and result in a better capacity for the second discharge cycle than for the first one. The peaks at 2.60 and 1.74 V of the first cathodic scan disappear in the following scans, implying a complete structural transition of $LiFe(MoO_4)_2$. Moreover, the structure evolution tends to stabilize after the initial cycle, as shown by the fifth CV curve's similarity to the second curve (Figure 3).

To examine the electrochemical kinetics behavior of the new anode $LiFe(MoO_4)_2$, GITT and EIS measurements are employed.[30] As shown in Figure 4, the GITT data of $LiFe(MoO_4)_2$ are collected at a current density of 56 mA g^{-1} and a time interval of 180 min. The average E_s value in the plateau region is smaller than 3 mV, which is approximated for the material to obtain a quasi-steady state. Assuming one-dimensional diffusion in a solid electrode on the basis of Fick's second law, the diffusion coefficient of Li$^+$ ($\tilde{D}_{Li^+}$) could be calculated using the formula[31]
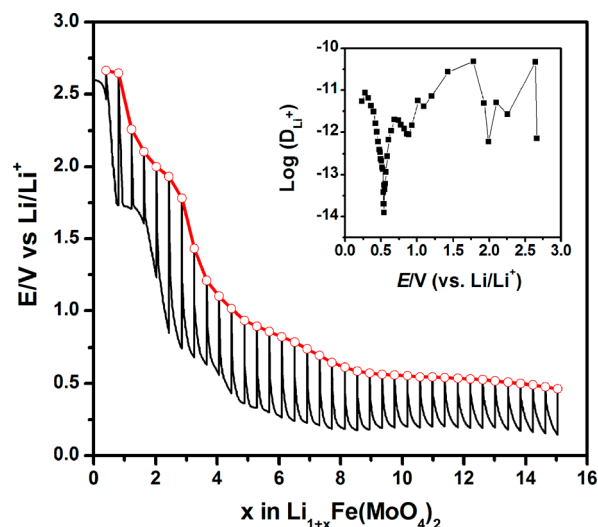

Figure 4. GITT data of $LiFe(MoO_4)_2$ collected at a current density of 56 mA g^{-1} and a time interval of 180 min. (Inset) Variation of $\tilde{D}_{Li^+}$ as a function of voltage in the first discharge.

$$\tilde{D}_{Li^+} = \frac{4}{\pi\tau}\left(\frac{m_B V_M}{M_B S}\right)^2\left(\frac{\Delta E_s}{\Delta E_\tau}\right)^2 \tag{1}$$

Where V_M (cm^2 s^{-1}), M_B (g mol^{-1}), m_B (g), and S (cm^2) are the molar volume, the molecular weight, the mass, and the active surface area, respectively. ΔE_τ and ΔE_s represent the total change of the cell voltage during the current pulse for the time τ and the change of the steady-state voltage of the cell for the step at plateau potential, respectively. The inset of Figure 4 shows the variation of $\tilde{D}_{Li^+}$ as a function of voltage in the first discharge. $\tilde{D}_{Li^+}$ is found to strongly depend on the electrochemical process, and the minimal $\tilde{D}_{Li^+}$ values in different stages correspond to the voltage plateaus of discharge process. Note that the steady voltages after being discharged in GITT measurement show a little difference from those in CV, which might come from the electrode polarization and different testing methods. The GITT technique is based on the chronopotentiometry, and its steady voltage is obtained after relaxation for a period of time, τ, while CV measurement focuses on the dynamic behavior of lithiation/delithiation in $LiFe(MoO_4)_2$.

As displayed in Figure 5, the Nyquist curves are obtained in the different stages of first discharge process, and the fitted equivalent circuits are inserted in Figure 5, where R_s is the series resistance of the electrodes, electrolyte, and the current collectors, R_f is the resistance of the SEI film, R_{ct} is the charge-transfer resistance between electrode/electrolyte interface, CPE is the constant phase element, and W is the Warburg impedance associated with the diffusion of the lithium ions. In the high-to-medium frequency region, the Nyquist plots of the open circuit and 1 Li$^+$ ion intercalation show one arc that corresponds to R_{ct} and can be well fitted by model 1 (Figure 5 inset). In contrast, two arcs contributed by R_f and R_{ct} and fitted by model 2 (Figure 5 inset) are obtained in the following Nyquist plots with more Li$^+$ ion insertion. The resistance parameters are calculated and listed in Table 1. R_f and R_{ct} are increasing at the initial intercalation due to the formation of SEI film. However, when 15 Li$^+$ ions are inserted into $LiFe(MoO_4)_2$, both R_f and R_{ct} decrease dramatically. This phenomenon has also been observed in other conversion-

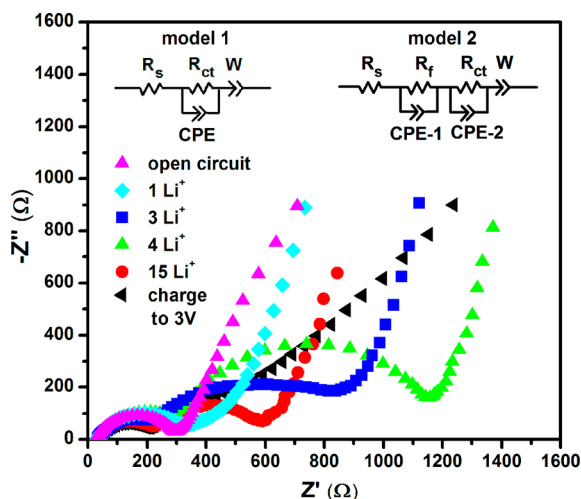**Figure 5.** Nyquist plots of $LiFe(MoO_4)_2$ obtained in the different stages of the first discharge process. (Inset) Two equivalent circuits used for fitting.

Table 1. Fitted Impedance Parameters of $LiFe(MoO_4)_2$ in the First Cycle State

	R_s (Ω)	R_f (Ω)	R_{ct} (Ω)
open circuit	27.99 ± 0.06		258.4 ± 2.1
1 Li	31.09 ± 0.10		274.8 ± 1.5
3 Li	33.38 ± 0.09	184.4 ± 2.1	470.1 ± 7.4
4 Li	35.74 ± 0.16	280.5 ± 4.3	843.9 ± 5.9
15 Li	37.01 ± 0.09	191.4 ± 1.3	299.7 ± 5.3
charge to 3 V	37.23 ± 0.11	162.9 ± 1.6	332.8 ± 10.9

type anodes[31] and might be attributed to the complete destruction of crystal structure and electrode particles.

It is necessary to investigate the lithium-ion storage mechanism of $LiFe(MoO_4)_2$ because it is a novel anode material. The theoretical capacity value for a fully discharged reaction of $LiFe(MoO_4)_2$ would involve a nearly 15 Li^+ ion reaction based on the conversion mechanism. To confirm the assumption, ex situ XRD was performed to study the Li^+ ion storage mechanism in the $LiFe(MoO_4)_2$ electrode, as shown in Figure 6. When the Li^+ ion is inserted into the $LiFe(MoO_4)_2$ in the initial discharge scan, the diffraction peaks broaden and shift, which is likely due to a structural transition under $P1$ symmetry, corresponding to the first discharge plateau at 2.56 V. Further increasing the content of Li^+ ions, the diffraction peaks at low angles ($2\theta < 30°$) disappear gradually and new peaks appear at 43.3° and 63.0°, indicating the emergence of a new phase. After the insertion of 4 Li^+ ions, the active material seems to develop a composite of Li_2MoO_3 and $Li_2Fe_3O_4$. With further lowering the potential voltage, more Li^+ ions are apt to be inserted into the Li_2MoO_3 and $Li_2Fe_3O_4$ lattices and form $Li_{2+x}MoO_3$ and $Li_{2+x}Fe_3O_4$, which are suggested to be the intermediate compounds of MoO_2 and Fe_3O_4 anodes in previous reports.[25,26,32] Moreover, when 15 Li^+ ions are inserted, several broad peaks appear instead of the sharp ones. The diffraction pattern after one discharge/charge cycle resembling that of the 15 Li^+ ion insertion indicates that structural transition completes after the first discharge process. Note that there are no obvious diffraction peaks of Mo and Fe metals when they are discharged to 0.01 V because of the broadened diffraction peaks, which can be attributed to the nanoparticle nature of electrochemically formed species.[23,33] A
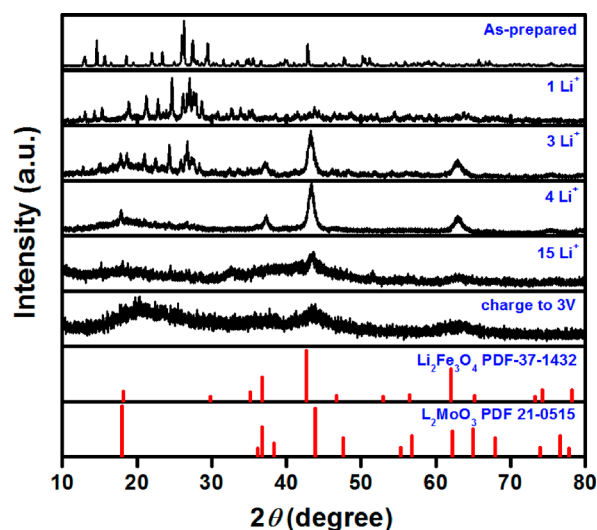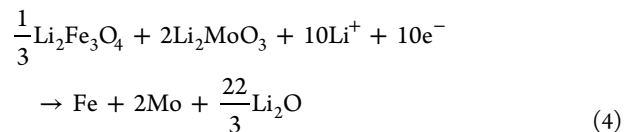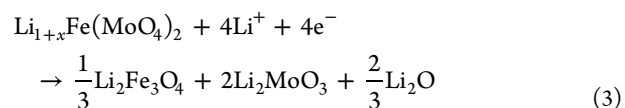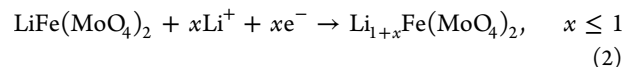

Figure 6. Ex situ XRD patterns of the $LiFe(MoO_4)_2$ electrode at different insertion/deinsertion stages during the first discharge and charge processes. Standard XRD patterns of $Li_2Fe_3O_4$ and Li_2MoO_3 are also shown as references.

similar situation has also been observed in the Fe_3O_4 and $ZnMn_2O_4$ anode materials.[23,33]

On the basis of the above analysis, a possible lithiation/delithiation mechanism of $LiFe(MoO_4)_2$ material in the first discharge process is proposed:

$$LiFe(MoO_4)_2 + xLi^+ + xe^- \rightarrow Li_{1+x}Fe(MoO_4)_2, \quad x \leq 1 \tag{2}$$

$$Li_{1+x}Fe(MoO_4)_2 + 4Li^+ + 4e^-$$
$$\rightarrow \frac{1}{3}Li_2Fe_3O_4 + 2Li_2MoO_3 + \frac{2}{3}Li_2O \tag{3}$$

$$\frac{1}{3}Li_2Fe_3O_4 + 2Li_2MoO_3 + 10Li^+ + 10e^-$$
$$\rightarrow Fe + 2Mo + \frac{22}{3}Li_2O \tag{4}$$

In addition, the microstructural evolution is also emphasized by HRTEM images of $LiFe(MoO_4)_2$ electrodes. To facilitate the observation of lattice fringes clearly, the Fourier filtering image is acquired by using in-plane Fourier spots, as depicted in the inset of Figure 7a. The crystalline region with clear lattice fringe has an interplanar spacing of about 0.41 nm, consistent with $(\overline{1}11)$ atomic planes of the triclinic structure. As shown in the inset of Figure 7b, the lattice fringes changes into 0.49 nm after 5 Li^+ ions are inserted, which corresponds to the (111) of Li_2MoO_3 or (111) of $Li_2Fe_3O_4$. The similarity in the crystal structure of Li_2MoO_3 and $Li_2Fe_3O_4$ makes it difficult to separate one from another as discussed in the ex situ XRD. Furthermore, a dislocation can also be observed as highlighted in red circles due to the lattice distortion induced by Li^+ ions insertion. When 15 Li^+ ions are inserted, a lattice fringe is hard to be detected due to the bad crystalline, SAED pattern at a relatively large scale, however, could verify the existence of Fe and Mo metal after being full discharged to 0.01 V through the conversion reaction. Similar Li-ion storage behavior has also been observed in nano-octahedrons-type $ZnFe_2O_4$ with the results of Zn and Fe metal particles evidenced by SAED.[34]
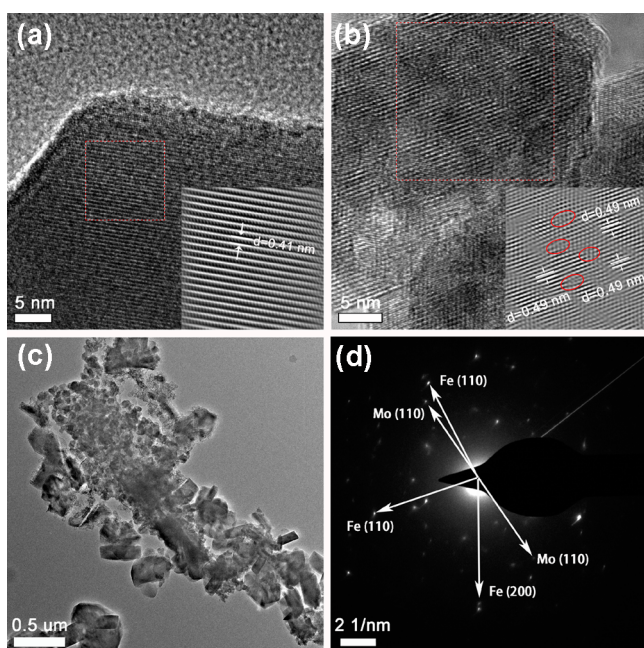
10664

dx.doi.org/10.1021/am502352c | *ACS Appl. Mater. Interfaces* 2014, 6, 10661−10666

Figure 7. HRTEM images of (a) the as-prepared material, (b) the anode material after 5 Li$^+$ ion insertion, (c) the anode material after 15 Li$^+$ ion insertion, (d) SAED pattern for the anode after 15 Li$^+$ ion insertion, and (insets) Fourier filtering images acquired by using in-plane Fourier spots.

LiFe(MoO$_4$)$_2$, for the first time, has been studied as anode in the voltage range between 3 and 0.01 V. A high discharge capacity of 1034 mAh g^{-1} is obtained after full discharge at a current density of 56 mA g^{-1}, suggesting nearly 15 Li$^+$ ions have been inserted, and Fe^{3+} and Mo^{6+} ions are correspondingly reduced into Fe and Mo, according to the conversion mechanism. Several cathode materials such as LiFePO$_4$ and Li$_2$FeSiO$_4$ have been treated as anode, and Li$_3$PO$_4$ and SiO$_2$ are found instead of P and Si.[12,13] The different resultants may come from the ability of Mo to exist in different oxidation states ranging from 0 to +6,[9] while P and Si usually show only one stable positive oxidation state of +5 and +4, respectively, and tend to form strong covalent bonds with oxygen via d–p hybridization. In the as-prepared LiFe(MoO$_4$)$_2$, Mo^{6+} ions with empty 4d orbitals can stabilize in the [MoO$_4$] tetrahedron and form a weak covalent bond. When discharged between 1.76 and 0.57 V, more than 2 Li$^+$ ions are inserted into the lattice, and electrons will induce the change of electronic state from Mo^{6+} into Mo^{4+}. This indicates the 4d orbitals of Mo^{6+} would be partly occupied, and the reduced ions have a definite octahedral-site preference,[21] which is manifested as a six-coordinated [MoO$_6$] octahedron in Li$_2$MoO$_3$. Hence, further lithiation would induce the decomposition of LiFe(MoO$_4$)$_2$ into Li$_2$MoO$_3$ and Li$_2$Fe$_3$O$_4$. Because Li$_2$MoO$_3$ and Li$_2$Fe$_3$O$_4$ have been found as the intermediate compounds for the MoO$_2$ and Fe$_3$O$_4$ anode materials,[25,26,32] at low potential (below 0.57 V), the anode could continue to be lithiated and reach a high discharge capacity.

CONCLUSION

Triclinic LiFe(MoO$_4$)$_2$ has been successfully synthesized by solid-state reaction. XRD and SEM are used to characterize the phase impurity and particle size. The LiFe(MoO$_4$)$_2$ electrode is found to deliver a high electrochemical capacity of 1034 mAh

g^{-1} at a current density of 56 mA g^{-1} after being fully discharged to 0.01 V. A reversible capacity of 580 mAh g^{-1} is maintained after 30 cycles. On the basis of the ex situ XRD and HRTEM results, the reaction mechanism involved in the lithiation/delithiation processes is proposed together with the charge/discharge curves and CV. Due to the multielectrons reaction nature, LiFe(MoO$_4$)$_2$ is expected to show a superior performance with modification of the preparation method or surface-coating in future studies.

AUTHOR INFORMATION

Corresponding Authors
*E-mail: dufei@jlu.edu.cn.
*E-mail: biexiaofei@yahoo.com.
Notes
The authors declare no competing financial interest.

ACKNOWLEDGMENTS

REFERENCES

(1) Armand, M.; Tarascon, J.-M. Building Better Batteries. *Nature* **2008**, *451*, 652−657.

(2) Cabana, J.; Monconduit, L.; Larcher, D.; Palacín, M. R. Beyond Intercalation-Based Li-Ion Batteries: The State of the Art and Challenges of Electrode Materials Reacting through Conversion Reactions. *Adv. Mater.* **2010**, *22*, E170−E192.

(3) Zhong, K. F.; Xia, X.; Zhang, B.; Li, H.; Wang, Z. X.; Chen, L. Q. MnO Powder as Anode Active Materials for Lithium Ion Batteries. *J. Power Sources* **2010**, *195*, 3300−3308.

(4) Ban, C. M.; Wu, A. C.; Gillaspie, D. T.; Chen, L.; Yan, Y. F.; Blackburn, J. L.; Dillon, A. C. Nanostructured Fe$_3$O$_4$/SWNT Electrode: Binder-Free and High-Rate Li-Ion Anode. *Adv. Mater.* **2010**, *22*, E145−E149.

(5) Lou, X. W.; Wang, Y.; Yuan, C. L.; Lee, J. Y.; Archer, L. A. Template-Free Synthesis of SnO$_2$ Hollow Nanostructures with High Lithium Storage Capacity. *Adv. Mater.* **2006**, *18*, 2325−2329.

(6) Seng, K. H.; Park, M.-H.; Guo, Z. P.; Liu, H. K.; Cho, J. Catalytic Role of Ge in Highly Reversible GeO$_2$/Ge/C Nanocomposite Anode Material for Lithium Batteries. *Nano Lett.* **2013**, *13*, 1230−1236.

(7) Wu, H. B.; Chen, J. S.; Hng, H. H.; Lou, X. W. Nanostructured Metal Oxide-Based Materials as Advanced Anodes for Lithium-Ion Batteries. *Nanoscale* **2012**, *4*, 2526−2542.

(8) Jiang, C. H.; Hosono, E.; Zhou, H. S. Nanomaterials for Lithium Ion Batteries. *Nano Today* **2006**, *1*, 28−33.

(9) Regalbuto, J. R.; Ha, J.-W. A Corrected Procedure and Consistent Interpretation for Temperature Programmed Reduction of Supported MoO$_3$. *Catal. Lett.* **1994**, *29*, 189−207.

(10) Lee, S.-H.; Kim, Y.-H.; Deshpande, R.; Parilla, P. A.; Whitney, E.; Gillaspie, D. T.; Jones, K. M.; Mahan, A. H.; Zhang, S. B.; Dillon, A. C. Reversible Lithium-Ion Insertion in Molybdenum Oxide Nanoparticles. *Adv. Mater.* **2008**, *20*, 3627−3632.

(11) Cherain, C. T.; Reddy, M. V.; Haur, S. C.; Chowdari, B. V. R. Interconnected Network of CoMoO$_4$ Submicrometer Particles as High Capacity Anode Material for Lithium Ion Batteries. *ACS Appl. Mater. Interfaces* **2012**, *5*, 918−923.

(12) Guo, X. W.; Fang, X. P.; Mao, Y.; Wang, Z. X.; Wu, F.; Chen, L. Q. Capacitive Energy Storage on Fe/Li$_3$PO$_4$ Grain Boundaries. *J. Phys. Chem. C* **2011**, *115*, 3803−3808.

(13) Xu, Y.; Li, Y. J.; Liu, S. Q.; Li, H. L.; Liu, Y. N. Nanoparticle Li_2FeSiO_4 as Anode Material for Lithium-Ion Batteries. *J. Power Sources* **2012**, *220*, 103−107.

(14) Lee, A.; Beaurain, M.; Armand, P. $LiFe(MoO_4)_2$, $LiGa(MoO_4)_2$, and $Li_3Ga(MoO_4)_3$. *Acta Crystallogr., Sect. C* **2008**, *64*, i1−i4.

(15) Devi, M.; Varadaraju, U. V. Lithium Insertion in Lithium Iron Molybdate. *Electrochem. Commun.* **2012**, *18*, 112−115.

(16) Jiang, T.; Wang, C. Z.; Chen, G.; Chen, H.; Wei, Y. J.; Li, X. Effects of Synthetic Route on the Structural, Physical, and Electrochemical Properties of $Li_3V_2(PO_4)_3$ Cathode Materials. *Solid State Ionics* **2009**, *180*, 708−714.

(17) Jiang, T.; Pan, W. C.; Wang, J.; Bie, X. F.; Du, F.; Wei, Y. J.; Wang, C. Z.; Chen, G. Carbon Coated $Li_3V_2(PO_4)_3$ Cathode Material Prepared by A PVA Assisted Sol−Gel Method. *Electrochim. Acta* **2010**, *55*, 3864−3869.

(18) Zhou, G. M.; Wang, D. W.; Li, F.; Zhang, L. L.; Li, N.; Wu, Z. S.; Wen, L.; Lu, G. Q.; Cheng, H. M. Graphene-Wrapped Fe_3O_4 Anode Material with Improved Reversible Capacity and Cyclic Stability for Lithium Ion Batteries. *Chem. Mater.* **2010**, *22*, 5306−5313.

(19) Muraliganth, T.; Murugan, A. V.; Manthiram, A. Facile Synthesis of Carbon-Decorated Single-Crystalline Fe_3O_4 Nanowires and their Application as High Performance Anode in Lithium Ion Batteries. *Chem. Commun.* **2009**, *47*, 7360−7362.

(20) Zhang, W. M.; Wu, X. L.; Hu, J. S.; Guo, Y. G.; Wan, L. J. Carbon Coated Fe_3O_4 Nanospindles as a Superior Anode Material for Lithium-Ion Batteries. *Adv. Funct. Mater.* **2008**, *18*, 3941−3946.

(21) Manthiram, A.; Goodenough, J. B. Lithium Insertion into $Fe_2(MoO_4)_3$ Frameworks: Comparison of M = W with M = Mo. *J. Solid State Chem.* **1987**, *71*, 349−360.

(22) Alvarez-Vega, M.; Amador, U.; Dompablo, M. E. A. Electrochemical Study of $Li_3Fe(MoO_4)_3$ as Positive Electrode in Lithium Cells. *J. Electrochem. Soc.* **2005**, *152*, A1306−A1311.

(23) Zhang, Q. M.; Shi, Z. C.; Deng, Y. F.; Zheng, J.; Liu, G. C.; Chen, G. H. Hollow Fe_3O_4/C Spheres as Superior Lithium Storage Materials. *J. Power Sources* **2012**, *197*, 305−309.

(24) Verma, P.; Maire, P.; Novák, P. A Review of the Features and Analyses of the Solid Electrolyte Interphase in Li-Ion Batteries. *Electrochim. Acta* **2010**, *55*, 6332−6341.

(25) Yoon, T.; Chae, C.; Sun, Y.-K.; Zhao, X.; Kung, H. H.; Lee, J. K. Bottom-Up in Situ Formation of Fe_3O_4 Nanocrystals in a Porous Carbon Foam for Lithium-Ion Battery Anodes. *J. Mater. Chem.* **2011**, *21*, 17325−17330.

(26) Li, W. Y.; Cheng, F. Y.; Tao, Z. L.; Chen, J. Vapor-Transportation Preparation and Reversible Lithium Intercalation/Deintercalation of α-MoO_3 Microrods. *J. Phys. Chem. B* **2006**, *110*, 119−124.

(27) Guo, B. K.; Fang, X. P.; Li, B.; Shi, Y. F.; Ouyang, C. Y.; Hu, Y.-S.; Wang, Z. X.; Stucky, G. D.; Chen, L. Q. Synthesis and Lithium Storage Mechanism of Ultrafine MoO_2 Nanorods. *Chem. Mater.* **2012**, *24*, 457−463.

(28) Chen, J.; Xu, L.; Li, W. Y.; Gou, X. L. α-Fe_2O_3 Nanotubes in Gas Sensor and Lithium-Ion Battery Applications. *Adv. Mater.* **2005**, *17*, 582−586.

(29) Ku, J. H.; Jung, Y. S.; Lee, K. T.; Kim, C. H.; Oh, S. M. Thermoelectrochemically Activated MoO_2 Powder Electrode for Lithium Secondary Batteries. *J. Eletrochem. Soc.* **2009**, *156*, A688−A693.

(30) Li, Z.; Du, F.; Bie, X. F.; Zhang, D.; Cai, Y. M.; Cui, X. R.; Wang, C. Z.; Chen, G.; Wei, Y. J. Electrochemical Kinetics of the $Li[Li_{0.23}Co_{0.3}Mn_{0.47}]O_2$ Cathode Material Studied by GITT and EIS. *J. Phys. Chem. C* **2010**, *114*, 22751−22757.

(31) Cao, Z. Y.; Wei, B. Q. High Rate Capability of Hydrogen Annealed Iron Oxide-Single Walled Carbon Nanotube Hybrid Films for Lithium-Ion Batteries. *ACS Appl. Mater. Interfaces* **2013**, *5*, 10246−10252.

(32) Hashem, A. M.; Askar, M. H.; Winter, M.; Albering, J. H.; Besenhard, J. O. Two-Phase Reaction Mechanism During Chemical Lithium Insertion into α-MoO_3. *Ionics* **2007**, *13*, 3−8.

(33) Deng, Y. F.; Tang, S. D.; Zhang, Q. M.; Shi, Z. C.; Zhang, L. T.; Zhan, S. Z.; Chen, G. H. Controllable Synthesis of Spinel Nano-$ZnMn_2O_4$ via a Single Source Precursor Route and its High Capacity Retention as Anode Material for Lithium Ion Batteries. *J. Mater. Chem.* **2011**, *21*, 11987−11995.

(34) Xing, Z.; Ju, Z. C.; Yang, J.; Xu, H. Y.; Qian, Y. T. One-Step Hydrothermal Synthesis of $ZnFe_2O_4$ Nano-Octahedrons as a High Capacity Anode Material for Li-Ion Batteries. *Nano Res.* **2012**, *5*, 477−485.

10666

dx.doi.org/10.1021/am502352c | *ACS Appl. Mater. Interfaces* 2014, 6, 10661−10666